Paleoceanography and Paleoclimatology

RESEARCH ARTICLE
10.1029/2023PA004821

Key Points:

- We present the first pairing of X-ray Micro CT scans and individual foraminiferal analyses of stable C and O isotopes
- CT Numbers generated from X-ray Micro CT scans of foraminifera are used as a dissolution proxy
- Drivers of dissolution and isotopic variation are decoupled over $\sim 10^3$ years timescales but are related over $\sim 10^5$ years timescales

Supporting Information:

Supporting Information may be found in the online version of this article.

Correspondence to:

D. Jana and M. Torres,
Debadrita.Jana@rice.edu;
mt61@rice.edu

Citation:

Jana, D., Torres, M., Evans, K., Jayan, A. K., & Thirumalai, K. (2024). Paired X-ray Micro CT scanning and individual foraminifera isotopic analysis reveal (de)coupled changes in carbonate preservation and temperature. *Paleoceanography and Paleoclimatology*, *39*, e2023PA004821. https://doi.org/10.1029/2023PA004821

Received 6 DEC 2023
Accepted 8 AUG 2024

Author Contributions:

Conceptualization: Debadrita Jana, Mark Torres
Formal analysis: Debadrita Jana
Investigation: Debadrita Jana, Ammoose K. Jayan
Methodology: Debadrita Jana, Mark Torres, Kory Evans, Kaustubh Thirumalai
Resources: Mark Torres, Kory Evans, Kaustubh Thirumalai
Software: Debadrita Jana, Mark Torres, Kory Evans
Supervision: Mark Torres, Kaustubh Thirumalai
Validation: Debadrita Jana
Writing – original draft: Debadrita Jana
Writing – review & editing: Mark Torres, Kaustubh Thirumalai

Paired X-Ray Micro CT Scanning and Individual Foraminifera Isotopic Analysis Reveal (De)coupled Changes in Carbonate Preservation and Temperature

Debadrita Jana[1], Mark Torres[1], Kory Evans[2], Ammoose K. Jayan[3], and Kaustubh Thirumalai[4]

[1]Department of Earth, Environmental and Planetary Sciences, Rice University, Houston, TX, USA, [2]Department of Ecology and Evolutionary Biology, Rice University, Houston, TX, USA, [3]Department of Geology, Central University of Kerala, Kasaragod, India, [4]Department of Geosciences, University of Arizona, Tucson, AZ, USA

Abstract The composition and preservation state of biogenic carbonate archives, such as foraminiferal tests, record ocean chemistry during the lifetime of the organism and post-depositional changes in ambient conditions via carbonate compensation. Depending upon the specific paleoclimate proxy, post-depositional processes, including dissolution, may alter original paleoenvironmental signals captured by the foraminifer's test composition. Accordingly, quantifying dissolution independent of geochemical measurements can improve proxy interpretation. Developing independent tools may also be useful for investigating whether changes in paleoclimatic conditions are associated with changes in seawater carbonate chemistry. Such approaches can be improved further if they are applied to individual foraminiferal tests, as specimen-to-specimen differences can record higher-frequency environmental changes compared to conventional bulk-scale analyses. Here, we combine individual foraminiferal carbon and oxygen isotopic analyses (IFA) with X-ray MicroCT Scanning to generate paired analyses of test density (a proxy for the extent of post-depositional dissolution) and isotopic composition. As a proof-of-concept application of this approach, we analyze *Globigerina bulloides* tests from both coretop and latest Miocene/earliest Pliocene-aged sediment from Ocean Drilling Project (ODP) Site 1088 (Agulhas Ridge). Our measurements and mixing model calculations show that within-population differences in carbon and oxygen isotopic ratios are largely independent of dissolution extent. By comparing population averages from coretop and downcore sediments, we find that lower oxygen isotopic ratios (likely driven by higher calcification temperatures) are associated with greater extents of dissolution at ODP Site 1088. We interpret this finding to reflect coupled changes in carbonate chemistry and climatic conditions over million-year timescales.

Plain Language Summary Foraminifera are microscopic marine protists that produce shells made of calcium carbonate. The chemical composition of these shells reflects the temperature and chemistry of the seawater in which they live. However, after foraminifera die, their shells may start to dissolve depending upon the depth of the seafloor they sink to and the local chemistry of the seawater. During dissolution, the chemical and physical composition of the calcium carbonate shell changes, impacting how we quantify past environmental conditions. Ideally, we would have some way of measuring how much each shell was dissolved to see which chemical analyses are affected and which are not. In this study, we used Micro CT scanning to measure how much dissolution individual shells of foraminifera experienced at the bottom of the ocean offshore of South Africa. By measuring the chemical composition of the exact same shells, we found that our specific measurements were unaffected by dissolution. However, we also found that ancient shells were more dissolved than modern shells, which likely reflects changes in ocean chemistry.

1. Introduction

Stable carbon and oxygen isotopic compositions of foraminiferal calcite have long been used to reconstruct past ocean-climate conditions such as temperature, salinity, carbonate chemistry, and ice volume, among other variables (Emiliani, 1955; Erez & Luz, 1983; Ravelo & Hillaire-Marcel, 2007; Scotese et al., 2021; Shackleton, 1987; Shackleton & Opdyke, 1973). Such measurements are typically performed on $CaCO_3$ powder obtained by crushing several tests, or shells, of planktic and benthic foraminifera, a procedure that approximates the average isotopic composition of all individuals within the given sample aliquot. As typical marine sediment samples can integrate sedimentation over 10^2–10^4 years, multiple-test foraminiferal analyses are typically used

for paleoceanographic reconstructions spanning timescales longer than 10^3 years. In contrast to the averaging imposed by commonly adopted sampling methods, the lifespan of planktic foraminifera is on the scale of weeks (Spero, 1998), and the pooled statistics of numerous individual shells analyzed from a sediment sample can reflect seasonal or multi-annual variation in climate-ocean parameters (Ford et al., 2015; Thirumalai & Clemens, 2020; Thirumalai & Maupin, 2023).

Many recent studies have utilized individual foraminiferal analyses (IFA) to measure "snapshots" of environmental conditions recorded during the short lifetime of an organism. In addition, IFA can also be used to resolve short-term climate signals such as the El Nino Southern Oscillation (ENSO), monsoonal cycles, and annual seasonal cycles (Ford et al., 2015; Glaubke et al., 2021; Thirumalai et al., 2013). In these and similar studies, isotopic variations of several permil (‰) have been observed in planktic foraminifera drawn from the same sediment aliquot, resulting partly from such high-frequency changes (Metcalfe et al., 2019; Sadekov et al., 2013) and partly from variation in metabolism and calcifying depth (Killingley et al., 1981) or calcification intensity (Spero & Lea, 1996) of each individual.

For both single and multispecimen foraminiferal analyses, the applicability of $\delta^{13}C$ and $\delta^{18}O$ values as reliable recorders of past ocean-atmosphere conditions assumes that these values reflect seawater conditions at the time when a living individual was actively calcifying. However, once foraminifera die and settle on the seafloor, they are acted upon by processes such as dissolution and recrystallization (Khider et al., 2011; Killingley et al., 1981). These processes can act over variable timescales and can impact primary test geochemistry. In addition to external environmental conditions, test ultrastructure and composition are important factors in the post-depositional fate of foraminiferal carbonate. For example, some experiments show that individual portions of tests, such as early-developed calcite (EDC), can preferentially dissolve (Iwasaki et al., 2015), which could drive overall changes in test composition provided sufficient differences in the chemistry of EDC compared to later forming phases (e.g., due to habitat migration; Lohmann, 1995). Other studies have shown genus-specific sensitivity of foraminiferal carbonate to dissolution (e.g., Clemens et al., 2023; Regenberg et al., 2014).

Dissolution of seafloor carbonates depends upon the ambient carbonate chemistry of the ocean (Zeebe & Wolf-Gladrow, 2001). Whereas deep marine carbonate burial accounts for the sequestration of ~300 Tg C/year (Hayes et al., 2021), it constitutes a small fraction of the total carbonate produced in the ocean. Various studies estimate that anywhere from 40% to 75% (Adkins et al., 2021; Feely et al., 2004; Milliman, 1993) of the $CaCO_3$ produced in the surface ocean is dissolved within the water column or at the seafloor (Broecker & Takahashi, 1978). The extent of carbonate dissolution within the ocean is controlled by the calcite saturation state of seawater, or Ω, which is expressed as:

$$\Omega = \left[Ca^{2+}\right]\left[CO_3^{2-}\right] / K^*_{sp} \quad (1)$$

where $[Ca^{2+}]$ and $[CO_3^{2-}]$ are the activities of calcium and carbonate ions in seawater, and K^*_{sp} is their solubility product. If Ω is much greater than 1, carbonates will be preserved within sediments, and at values of Ω less than or close to 1, they will dissolve (Zeebe & Wolf-Gladrow, 2001). The carbonate ion concentration of the ocean is ultimately modulated by atmospheric CO_2 levels on timescales of 10^3–10^5 years (Hönisch et al., 2012). Specifically, increasing levels of atmospheric CO_2 lowers the carbonate ion concentration of the ocean, which leads to a reduction in Ω and drives the dissolution of seafloor carbonates (Boudreau et al., 2018).

X-ray Micro Computed Tomography Scanning (hereafter referred to as XMCT) has emerged as a valuable technique to study the intensity and effects of test dissolution in foraminifera (Iwasaki et al., 2015, 2019, 2023; Johnstone et al., 2010, 2011; Zarkogiannis et al., 2022). This technique is based on the physical relationship between the density of a material and the attenuation of X-rays passing through it. Dissolution leads to a reduction in test density resulting from increased microporosity (Iwasaki et al., 2015, 2019; Johnstone et al., 2011; Volbers & Henrich, 2002).

Based on the concept of greater attenuation of X-rays while passing through denser parts of the test, Iwasaki et al. (2015) used the CT Number as a proxy for foraminiferal test density:

$$\text{CT Number} = \left[\left(\mu_{sample} - \mu_{air} \right) / \left(\mu_{standard} - \mu_{air} \right) \right] * 1{,}000 \quad (2)$$

where μ_{sample}, $\mu_{standard}$, and μ_{air} are the X-ray attenuation coefficients of the sample, a standard with known density, and air, respectively. Based on Equation 1, samples with higher density have higher CT Numbers, and those with lower density are characterized by lower CT Numbers. Given the high resolution of available instruments (~4 microns per voxel), each 3D scan of individual foraminifera comprises many measurements of CT Numbers that reflect intra-test heterogeneity in density.

In their dissolution experiments, Iwasaki et al. (2015) observed characteristic changes in the shape of the distribution of CT Numbers as shells were progressively dissolved. As a simple way to capture the first-order effect of changes in distribution shape with increasing dissolution extent, the percentage of foraminiferal calcite that has a CT number less than a given threshold can be used:

$$\%\text{Low-CT-number calcite volume} = (V_{\text{low-CT-number calcite}} / V_{\text{whole shell}}) * 100 \quad (3)$$

where $V_{\text{low-CT-number calcite}}$ is the volume of low-CT-number (i.e., CT Number is less than a defined threshold) calcite in an individual test, and $V_{\text{whole shell}}$ is the volume of the whole individual (Iwasaki et al., 2019). In addition to showing a relationship with dissolution extent in laboratory experiments (Iwasaki et al., 2015), %Low-CT-number calcite volume of foraminifera collected from core-top sediment shows a negative correlation with the local seawater $\Delta[CO_3^{2-}]$, which is the difference between the concentration of carbonate ion expected at saturation with respect to calcite in the modern ocean and the observed value.

Besides dissolution, other factors may influence the microporosity of foraminiferal carbonate and thus the expected CT distribution, for example, temperature, water density, salinity, dissolved oxygen, or nutrient concentrations (Burke et al., 2018; Davis et al., 2021; Glock et al., 2011; Kuroyanagi et al., 2013; Zarkogiannis et al., 2022). As a potential way to account for any intra-sample differences in initial CT Numbers associated with these factors, Iwasaki et al. (2023) scaled each individual CT Number measurement of a single foraminifera by the maximum value from that sample:

$$CT_{i,\text{scaled}} = (CT_i / CT_{\text{max}}) * 100 \quad (4)$$

where CT_i is the CT Number of any scanned volume, CT_{max} is the largest CT Number calculated in that individual, and $CT_{i,\text{scaled}}$ is the value of the CT Number obtained after scaling.

Whereas available studies have used XMCT to trace the process and effects of dissolution on foraminiferal tests (Iwasaki et al., 2015, 2019, 2023; Johnstone et al., 2010, 2011), coupling this proxy with geochemical measurements to simultaneously track changes in other environmental conditions (e.g., temperature; Johnstone et al., 2011) is less common. Moreover, past efforts have compared XMCT data acquired for individual tests to bulk geochemical measurements of multiple individuals (e.g., Johnstone et al., 2011; Iwasaki et al., 2023) instead of utilizing IFA to address geochemical variation between specimens obtained from the same sedimentary sample. To address both the physical and geochemical alteration of individual foraminifera and its implications for paleoclimate interpretations, we performed paired XMCT and IFA-$\delta^{18}O$ measurements on single tests of the planktic foraminifer *Globigerina bulloides* from both coretop and downcore (latest Miocene-earliest Pliocene aged) sediments.

G. bulloides is a spinose, non-symbiotic planktic foraminiferal species that resides within the upper water column between ~50 and 100 m (Figure 1b) and has an affinity for relatively cooler temperatures (Hemleben et al., 2012; SenGupta, 2002). *G. bulloides* juveniles calcify at warmer surface waters (Schiebel et al., 1997) and spend the latter part of their life cycle in deeper, cooler waters within the thermocline (Hemleben et al., 2012). Although they have a global distribution, they are most abundant at middle-high latitudes and upwelling zones (Bé & Hamlin, 1967) and show strong seasonality (Jonkers et al., 2013; King & Howard, 2005; Pak et al., 2004). Based on mass loss experiments conducted under controlled pH over increasing durations of time (Bé et al., 1975), *G. bulloides* was found to be a dissolution-prone species of planktonic foraminifera. *G. bulloides* tests are made up of multiple layers of calcite that may be classified into three categories (Iwasaki et al., 2015): Early Developed Calcite (EDC) and two types of Later Developed Calcite (LDC). EDC forms during the juvenile stage and constitutes the first 8–9 chambers. This material is composed of anhedral calcite and displays the lowest CT Numbers. LDC forms during later life stages and consists of an inner layer with intermediate CT numbers and a euhedral outer layer, which has the highest CT numbers within a test.

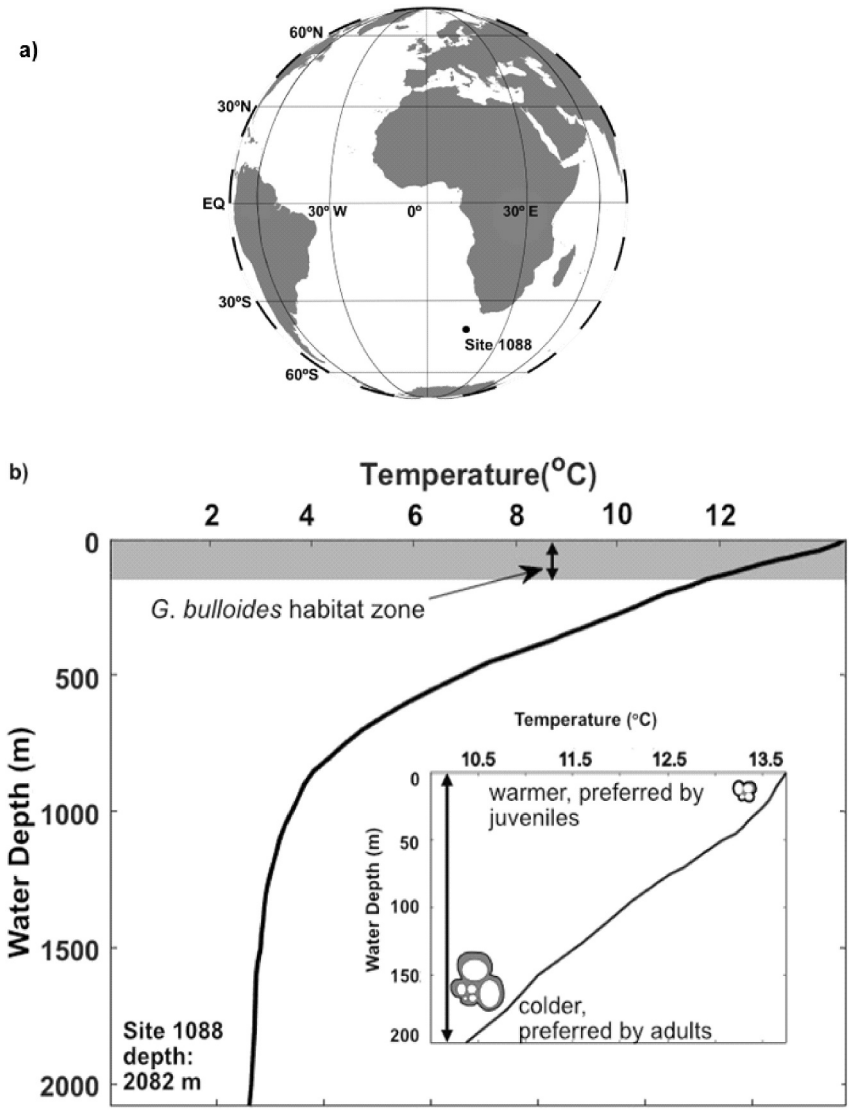

Figure 1. (a) Location of Site 1088 (b) Temperature profile at Site 1088 (2,082 mbsl depth) with the habitat zone of *G. bulloides* denoted in gray (Prasanna et al., 2016). The inset figure shows the temperature profile of the *G. bulloides* depth habitat. Juvenile *G. bulloides* prefer warmer surface waters (Schiebel et al., 1997), while the adults prefer colder water at greater depths (Hemleben et al., 2012).

Past dissolution experiments suggest that EDC is preferentially removed during dissolution (Iwasaki et al., 2015). Given data showing inter-shell differences in carbon and oxygen isotopic ratios (Lohmann, 1995; Spero & Lea, 1996), there is the potential for partial dissolution to influence the overall isotopic composition of a foraminiferal test. Here, we aim to test for dissolution effects on C and O isotopic ratios by pairing XMCT and IFA. If present, we hypothesize that a dissolution effect would manifest as a correlation between %Low-CT-number calcite volume and either $\delta^{13}C$ or $\delta^{18}O$. An absence of a correlation would imply a negligible impact of dissolution but also raise the question about the utility of paired XMCT and IFA: if dissolution does not affect $\delta^{13}C$/$\delta^{18}O$, is it worth the effort to quantify dissolution using XMCT? To highlight the utility of paired XMCT and IFA, independent of testing the fidelity of existing geochemical proxies, we leverage the fact that dissolution extent is reflective of ambient carbonate chemistry near the seafloor (Iwasaki et al., 2019) and test for correlations between paleo-temperatures (using $\delta^{18}O$) and carbonate chemistry (using XMCT) over geologic timescales.

2. Sites and Samples

Tests of *G. bulloides* were picked from sediments recovered from ODP Leg 177 Site 1088 (Figure 1a). Site 1088 (41°S, 15°E) is located on the Agulhas Ridge, a bathymetric high in the sub-Antarctic Southern Ocean. The lithology at this site mainly consists of Holocene to Middle Miocene carbonate ooze ($CaCO_3$ > 85%–95%), dominated by varying proportions of nannofossils and foraminifera (Gersonde et al., 1998).

At present, Site 1088 lies just south of the Subtropical Front (STF) at a depth of 2,082 mbsl (Figure 1b). This puts the site at the junction of the nutrient-rich, [CO_3^{2-}]-poor Circumpolar Deep Water (CDW) from the high-latitude Southern Ocean; and the nutrient-poor, [CO_3^{2-}]-rich North Atlantic Deep Water (NADW) from the high-latitude Atlantic Ocean (Billups, 2002; Gersonde et al., 1998). Subantarctic Surface Water (SASW) constitutes the surface current in this region, and it is underlain by the Antarctic Intermediate Water (AAIW). The oceanography in this region is also influenced by the presence of Agulhas rings, which are anticyclonic rings shed by the southward flowing Agulhas Current as it returns eastwards into the Indian Ocean (van Sebille et al., 2009, 2015). This is also a region of strong bottom water current activity, where seafloor sediments can be entrained and eroded based on current strength (Gruetzner et al., 2016).

For this study, we have adopted the age model outlined by Herbert et al. (2016), which is based on calcareous nannofossil biostratigraphy and oxygen isotope stratigraphy of Site 1088 (Gersonde et al., 1998; Hodell et al., 2003; Marino & Flores, 2002). For this study, we obtained two samples, namely Sample1088B-1H-1 (0.3 mbsf) and Sample 1088B-6H-5 (50.1 mbsf). Based on a sedimentation rate of ∼10.87 m/Myr near the coretop, the age of the first sample is calculated to be 0.02 ka (±5ka). Further down the section, the sedimentation rate is ∼5.17 m/Myr between the depths of 48.6 and 51.4 mbsf. The age of our downcore sample is calculated to be 5.29 Ma (±100 ka), which places it at the transition between the Miocene and Pliocene.

Our target species, *G. bulloides*, is an abundant taxon at Site 1088. Temperature-$\delta^{18}O$ calibrations established for *G. bulloides* take into account enrichment in oxygen isotopic compositions due to increasing depth of calcification as more chambers are added in later life stages (Bemis et al., 1998). However, isotopic measurements of *G. bulloides* collected in plankton tows along a Southern Ocean transect (Prasanna et al., 2016) do not conform to the temperature-$\delta^{18}O$ relationships established at lower latitudes. Likely, this discrepant behavior of *G. bulloides* at high latitudes is due to vital effects, the exact nature of which are not fully understood (Prasanna et al., 2016). Ultimately, these observations complicate *G. bulloides*-based temperature reconstructions in high latitudes, at least in terms of absolute values. Despite such discrepancies, $\delta^{18}O$ values of diachronous populations of *G. bulloides* reflect long-term changes in upper ocean temperatures, assuming that vital effects observed in these foraminifera at southern high latitudes do not vary appreciably over time (Veizer & Prokoph, 2015).

3. Materials and Methods

3.1. Sample Preparation

Sediments from both the core intervals were wet-sieved over a 150 μm sieve and oven-dried at 55°C overnight. Individual tests of *G. bulloides* were picked from the >150 μm size fraction and gently brushed with the wet tip of a paintbrush to remove any adhering clay. Broken or partially fragmented tests were avoided. Nearly all *Globigerina bulloides* larger than 150 μm produce a crust of gametogenic calcite (Hemleben et al., 2012). So, we assume that most, if not all, of the measured foraminifera have the gametogenic calcite crust. A Scanning Electron Micrograph of a calcite crust observed on an individual is shown in Figure S1 in Supporting Information S1.

3.2. X-Ray Micro CT Scanning

For each XMCT analytical run, about 25–50 individuals were mounted on a 1.2 cm × 1 cm cardboard sample holder using double-sided carbon tape prior to scanning. Mounted foraminifera were imaged on a Bruker Skyscan 1272 Micro-CT Scanner at the Department of Ecology and Evolutionary Biology at Rice University. The samples were scanned without any filter at a voltage of 80 kV, current strength of 80 μA, and stage rotation set at incremental steps of 0.15°. The exposure time for each step was set at 30 ms. The total runtime was about 2 hr for each mount bearing multiple individuals. To account for subtle variations in the physical properties of the sample mounts or scanning conditions, a crystal of the calcite standard IAEA 603 was imaged with every run. In total, 123 individuals from the coretop sample and 88 individuals from the downcore sample were scanned.

Post scanning, images were reconstructed using the nRecon software package (developed by Bruker Corporation, 2024). 3D volume rendering was performed using the open-source software package 3D Slicer (Fedorov et al., 2012), which is freely available at http://www.slicer.org. Individual foraminiferal volumes were isolated and saved as .nrrd files, after which they were processed using the Image Processing Toolbox in MATLAB R2023a. Specifically, standardized CT Numbers were calculated using Equation 2 and the observed attenuation of the IAEA 603 standard. Additionally, CT Numbers less than 200 were removed to avoid any possible influence of the sample holder or surrounding air.

After CT Numbers are calculated using Equation 2 and scaled using Equation 4, CT Number maps, which are cross-sectional slices across each test, were generated. These maps illustrate the spatial variation of CT Numbers within each individual.

CT Number distributions were also generated using kernel density estimation to represent the overall intra-test variation in CT Numbers (Figures 3c, 3f, 3i, and 3l). Shapes of CT Number distributions are used as an indicator of dissolution intensity, as demonstrated by the dissolution experiments of Iwasaki et al. (2015). Examples of CT Number distributions generated without and with scaling between 0 and 100 are shown in Figure 2. Prior to dissolution, the CT Number distributions of pristine foraminiferal tests show unimodal left-skewed distributions with peaks at high CT Numbers (Iwasaki et al., 2015). At the initial stages of dissolution, the relative proportions of low CT Numbers within the tests increase, giving rise to bimodal CT Number distributions. As dissolution progresses further, the distribution peaks exhibit a distinct shift to lower CT Numbers, thus forming unimodal right-skewed shapes that characterize highly dissolved tests.

The %Low-CT-number calcite volume was calculated using Equation 3, and the threshold for "Low" CT Numbers was set at 50 following Iwasaki et al. (2023). Additionally, we calculated the %Low-CT-number calcite volume using 40 and 60 as the Low CT Number threshold. This allows us to determine whether the Low CT Number threshold has an effect on relationships between the dissolution intensity and isotopic compositions of tests.

A peak-counting function (findpeaks) in the Signal Processing Toolbox in MATLAB was used to determine whether the CT Number distributions are unimodal, bimodal, or have more than two modes. The peak-counting results were compared visually with the distributions to check for correctness.

3.3. SEM Imaging

Specimens of *G. bulloides* were picked from each of the coretop ($n = 7$) and downcore ($n = 6$) samples based on their mean CT Numbers and the shapes of their CT Number distributions. These tests were then imaged using a FEI Quanta 400 ESEM under low vacuum settings to observe whether characteristic shapes of their CT Number distributions correspond to visible expressions of test alteration.

3.4. Individual Foraminiferal Analysis (IFA) for C and O Isotopes

Stable carbon ($\delta^{13}C$) and oxygen ($\delta^{18}O$) isotopic compositions of individual foraminifera were measured using a Kiel Carbonate Device IV coupled to a Thermo Fisher MAT 253 Plus Isotope Ratio Mass Spectrometer (IRMS) housed in the Paleo^2 Laboratory in the Department of Geosciences, University of Arizona. All individuals were weighed on a Sartorius ultramicrobalance prior to analysis, and only samples with mass >10 μg were analyzed in accordance with the long-term precision setup of analyzing small quantities of carbonates on this machine (Thirumalai et al., 2023). Individual foraminiferal tests were acidified with supersaturated (105%) phosphoric acid in the Kiel Carbonate Device, upon which sample CO_2 released is dehydrated and passed into the IRMS to measure isotopic ratios. The IFA data set in this study consists of $\delta^{13}C$ and $\delta^{18}O$ values of 90 foraminifera (67 coretop and 23 downcore individuals). Correlations between %Low-CT-number calcite volume and stable isotopic compositions were calculated using both ordinary least squares regression and a MATLAB package (Thirumalai et al., 2011) that uses a weighted least-squares method to fit a straight line to points having uncertainty in both x- and y-variables. The uncertainty in %Low-CT-number calcite volume was calculated as the difference in %Low CT Number Calcite volume calculated for the different thresholds of 40 and 60 (see above). The uncertainty in $\delta^{13}C$ and $\delta^{18}O$ are 0.07‰ and 0.08‰, respectively, which are the uncertainties associated with our IFA measurements.

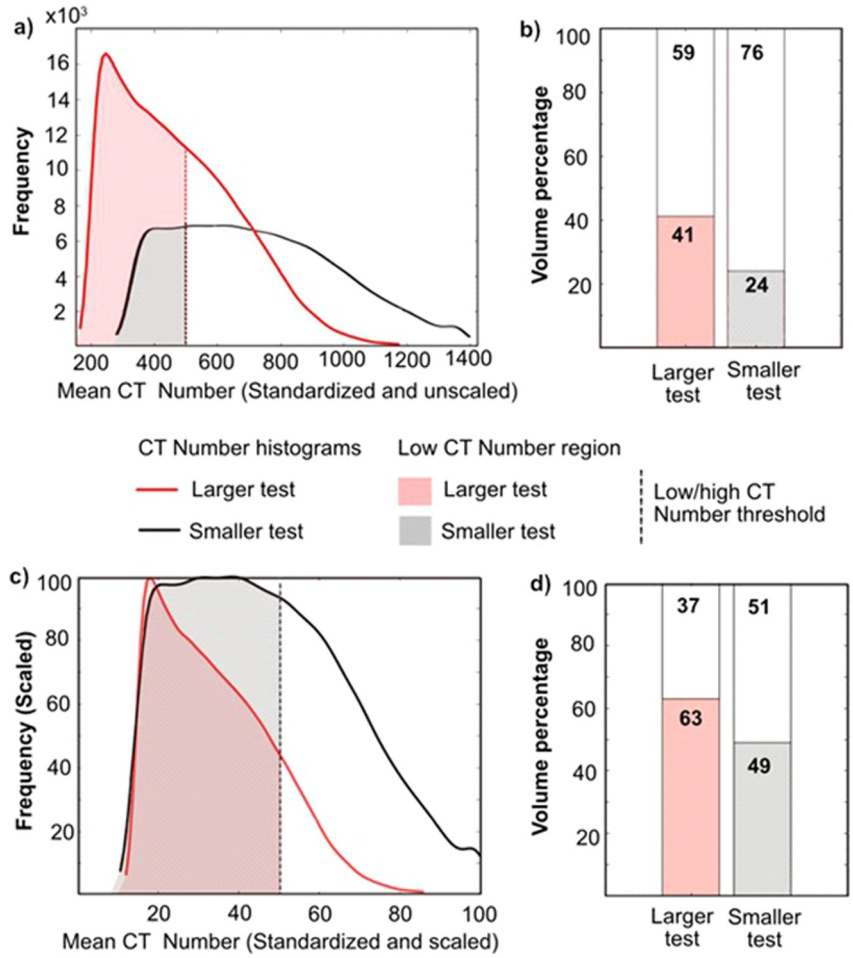

Figure 2. Examples of CT Number distributions generated by normalizing raw X-ray attenuation coefficients normalized with respect to a standard (a) and scaling the values between 0 and 100 to remove the effects of variable test size (c). (b, d) Show stacked bar charts showing the %Low-CT-number calcite volume, or the percentage of foraminiferal calcite that has a CT number less than a given threshold. Since our analysis makes use of 3D scans, we label it as a volume percentage. The effect of scaling on %Low CT Number Calcite volume is shown in (d). The threshold for Low CT Numbers is set at 50 for all four figures.

4. Results

4.1. CT Number Maps and Distributions

In our scans, *G. bulloides* individuals from both the coretop and downcore populations show that the highest CT Number (warmer colors in Figure 3, middle panel) are most common on the walls of the larger outer chambers. This matches the scans from Iwasaki et al. (2015), where the euhedral, dissolution-resistant layer of later developed calcite (LDC, also described as the "outer calcite") had the highest CT Numbers both before and after the dissolution experiments were performed. This layer is most abundant in the outermost chambers of the tests. Lower CT Numbers (cooler colors in Figure 3, middle panel) are more common in the smaller, earlier developed inner chamber walls.

A few examples of intra-test variation of CT Numbers and the shapes of the corresponding CT Number distributions are shown in Figure 3. The individual shown in Figures 3a–3c has a CT Number distribution with a single broad peak (Figure 3c), slightly skewed to the left, which is indicative of partial dissolution (Iwasaki et al., 2015). In comparison, the individual shown in Figures 3d–3f is also characterized by a left-skewed distribution (Figure 3f), but with a larger proportion of lower CT Numbers indicating a greater degree of dissolution compared to the individual in Figures 3a–3c. This interpretation of the CT distributions matches the SEM images, which, for

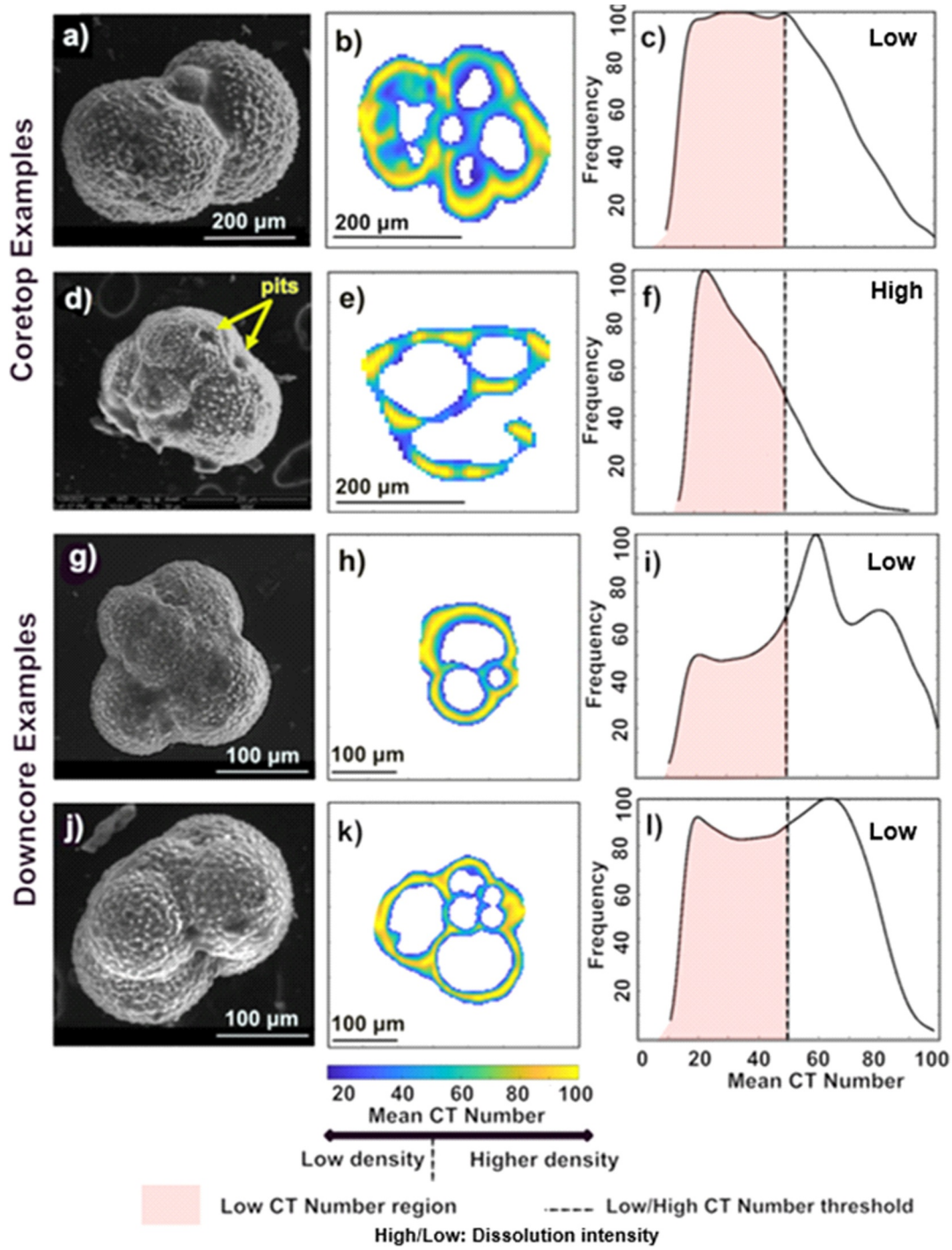

Figure 3. (left panel) (a, d, g, j) SEM images, Center panel (b, e, h, k): CT Number distribution map, and Right panel (c, f, i, l): CT Number distributions of individuals drawn from the coretop population. Panel (f) shows the characteristic shape of an individual that has undergone a high degree of dissolution, while panels (c, i, l) are examples of individuals that are better preserved.

the individual shown in Figure 3d, highlights large pits and other, more visible signs of dissolution. The individual shown in Figures 3g–3i has a CT Number distribution containing three peaks (Figure 3i), with the highest being at CT Number ~59, followed by peaks at CT Numbers 80 and 19, respectively. The individual in Figures 3j–3l has a bimodal CT Number distribution (Figure 3l), with the larger peak at CT Number ~64, and a slightly smaller peak

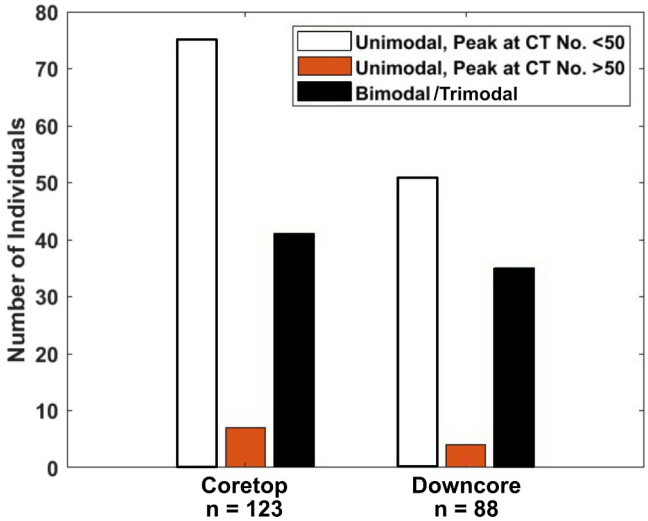

Figure 4. Classification of CT Number distributions from both the Coretop and Downcore populations based on the number and position of peaks.

at CT Number ~19. The individuals in Figures 3a–3c, 3g–3i, and 3j–3l each represent better degrees of preservation compared to Figures 3d–3f.

The qualitative analysis of CT Number distributions described above presupposes that the distributions are statistically different from one another. To confirm this, we used Two-sample Kolmogorov-Smirnov (ks) tests performed on each possible pair of whole-shell CT Number data sets for both the coretop and downcore individuals shown in Figure 3. In each case, we can reject the null hypothesis that the data are from the same continuous distribution (Table S1 in Supporting Information S1).

Out of the 123 scanned coretop individuals, CT number distributions in 66% (82 individuals) are unimodal, and the majority of these (75 individuals) are left-skewed with modes lying at CT Numbers <50. The remaining 41 individuals have bimodal CT Number distributions; the larger peak mostly lies in the Low CT Number (<50) region (Figure 4). In the downcore batch, 59% (51 individuals) have unimodal CT Number distributions with modes in the Low CT Number (<50) region. Modes at higher CT Numbers are observed in only four samples. The remaining 41% (35 individuals) have more than one peak in their CT number distributions, out of which 27 individuals have bimodal, and eight individuals have trimodal. In the bimodal distributions, the larger peaks lie mostly in the Low CT Number Region.

For each individual in both the core top and downcore populations, we calculated a mean and median CT Number as well as the %Low-CT-number calcite volume. Mean CT Numbers for the coretop batch range from 31 to 58 and, for the downcore batch, range from 28 to 60. The %Low-CT-number calcite volume ranges from ~46% to 89% for coretop samples and from ~41% to 90% for downcore samples. The XMCT-derived data for both the coretop and downcore populations are summarized in Table 1.

4.2. Individual Foraminiferal Analyses (IFA)

Stable carbon and oxygen isotope IFA show that $\delta^{18}O$ values are higher in the coretop population, whereas the ranges of $\delta^{13}C$ values for coretop and downcore specimens overlap (Figure 5). Specifically, $\delta^{13}C$ values in coretop samples range from −1.08‰ to 1.62‰ and in downcore samples range from −0.77‰ to 0.94‰. $\delta^{18}O$ in coretop samples ranges from 0.44‰ to 4.15‰. In downcore samples, the $\delta^{18}O$ has a narrower range from 0.27‰ to 1.60‰. The coretop samples have larger ranges for both $\delta^{13}C$ and $\delta^{18}O$ than the downcore samples. Visually, the coretop and downcore populations form two distinct groups when their $\delta^{13}C$ versus $\delta^{18}O$ values are plotted against each other (Figure 5). The IFA data measured on both the coretop and downcore populations are summarized in Table 1.

Table 1
%Low CT Number Calcite Volume, $\delta^{13}C$ and Measured on the Coretop (a) and Downcore (b) Populations

	Min	Max	Mean	Median	SD
(a) Coretop population statistics					
%Low-CT-number calcite volume	0.46	0.89	0.62	0.60	0.1
$\delta^{13}C$	−1.62	1.08	−0.25	−0.19	0.498
$\delta^{18}O$	0.44	4.15	2.63	2.73	0.62
(b) Downcore population statistics					
%Low-CT-number calcite volume	0.40	0.90	0.69	0.71	0.13
$\delta^{13}C$	−0.95	0.94	0.28	0.303	0.48
$\delta^{18}O$	0.29	1.8	0.97	0.95	0.38

Note. The mean and median values of each population are considered as "bulk" values, representative of the entire population.

We find that the %Low-CT-number calcite volume and both $\delta^{13}C$ and $\delta^{18}O$ are uncorrelated using both types of regression models (ordinary least squares and York regression; Thirumalai et al., 2011). For simplicity, we only discuss the results using ordinary least squares in the main text. The r^2 values for the linear regressions of $\delta^{18}O$ and the %Low-CT-number calcite volume were <0.01 for the coretop (Figure 6a) and <0.1 downcore populations (Figure 6b). Similarly, the correlation coefficients between $\delta^{13}C$ and %Low-CT-number calcite volume were <0.01 for the coretop (Figure 7a) and 0.05 for the downcore populations (Figure 7b), respectively. The statistical parameters describing the simple linear regression fit to the XMCT versus IFA data set for coretop and downcore populations are summarized in Tables 2 and 3. Weighted linear regression fits to the XMCT versus IFA data set for both the coretop and downcore populations are presented in Text S1 in Supporting Information S1 (Figures S4, S5, and Table S3).

These correlations were established using values of %Low CT Number Calcite Volume calculated using Equations 2–4, where the threshold of Low

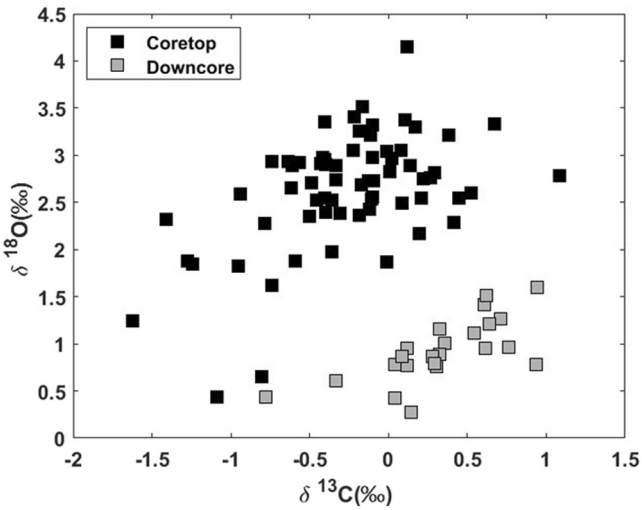

Figure 5. $\delta^{13}C$ and $\delta^{18}O$ measured through individual foraminiferal analysis (IFA) form two separate populations with distinct correlation statistics for both the coretop ($r^2 = 0.27$, $p > 0.1$ for a simple linear regression model) and downcore ($r^2 = 0.05$, $p > 0.1$ for a simple linear regression model) data sets. Detailed correlation statistics for simple and weighted linear regressions fit to these data sets are provided in Table S2 (Text S1 in Supporting Information S1).

CT Numbers was set at 50. %Low CT Number Calcite Volume was also calculated with the Low CT threshold set at 40 and 60, and no correlation was found between these values and $\delta^{18}O$ (see Figure S6 and Table S4 in Supporting Information S1).

5. Discussion

In this work, we apply a new approach that pairs X-ray Micro CT scans and stable carbonate isotopic measurements of individual foraminifera to generate data sets of test density, $\delta^{13}C$, and $\delta^{18}O$. We apply this technique to two populations of foraminifera: one coretop sample (0.3 mbsf; approximately modern) and one downcore sample (50.1 mbsf; 5.29 Ma) at ODP Site 1088 in the sub-Antarctic Southern Ocean. Individual foraminifera from each population record changes in environmental conditions occurring over ~900–1,900 years (see section on age model in Site and Samples), and thus inter-population differences yield insights into how climate variability within these intervals was different and/or how post-depositional alteration influences test structure and isotopic composition. By comparing data from the modern and downcore populations, we are additionally able to investigate how longer-term changes in oceanographic conditions are reflected in the structural and compositional changes of foraminiferal tests.

5.1. Interpretation of XMCT in Terms of Partial Dissolution Extent

Our XMCT data provide evidence of differences in mean densities (as CT Number) and variable density distributions (Figure 3) between individual scanned *G. bulloides* tests from the same sediment sample. Past work (Iwasaki et al., 2015, 2019, 2023; Johnstone et al., 2010, 2011; Zarkogiannis et al., 2022) has linked such differences to the extent of partial test dissolution in both *G. bulloides* as well as other foraminifera. In contrast, some recent studies have shown that ambient environmental conditions such as temperature (Burke et al., 2018) and dissolved oxygen levels (Davis et al., 2021; Kuroyanagi et al., 2013) can influence test porosity, and in turn, density. For our sample set, we argue that the observed differences in shapes of CT distributions are largely due to varying extents of partial dissolution as opposed to alternative ambient environmental factors.

The examples of characteristic CT Number distribution shapes observed in this study, as shown in Figure 3, largely match prior XMCT measurements of the same foraminiferal species (Iwasaki et al., 2015). We find that right-skewed shapes (e.g., Figure 3f) are the most common in our data set (Figure 4), and we interpret these as indicators of high degrees of dissolution in most of the scanned specimens. This is further supported by the SEM image in Figure 3d, where diagnostic markers of dissolution, such as pits or enlarged pores, are observed on the test surface of an individual from the coretop population and are accompanied by a right-skewed CT number distribution in Figure 3f. Most of the bimodal CT Number distributions have the more prominent peak in the lower CT Number region, Figure 3c being an example. This is a sign of the early stages of dissolution (Iwasaki et al., 2015), where a gradual decrease in the modes of CT Number distributions results from progressive dissolution, causing an increase in test porosity and a decrease in calcite CT Numbers. The distributions with peaks in the high CT Number region (e.g., Figure 3l) are consistent with the distributions of the initial phase of the experiments with no or little alteration. Corresponding SEM images of the individuals with bimodal CT Number distributions do not show prominent dissolution features.

5.2. Partial Dissolution Extent Does Not Drive Changes in IFA Oxygen Isotopic Ratios

The lack of correlation between %Low-CT-number calcite volume and $\delta^{18}O$ observed in both core-top (Figure 6a) and down-core populations (Figure 6b) suggests carbonate density variations and temperature signals are largely unrelated in these samples at the level of individual populations. This suggests that the dissolution process alone is insufficient to drive the differences in isotopic ratios we observe between these samples. This interpretation is consistent with simple mixing model calculations (Supporting Information S1) for the potential change in $\delta^{18}O$ as a result of dissolution, assuming that EDC dissolved preferentially and is characterized by lower $\delta^{18}O$ compared

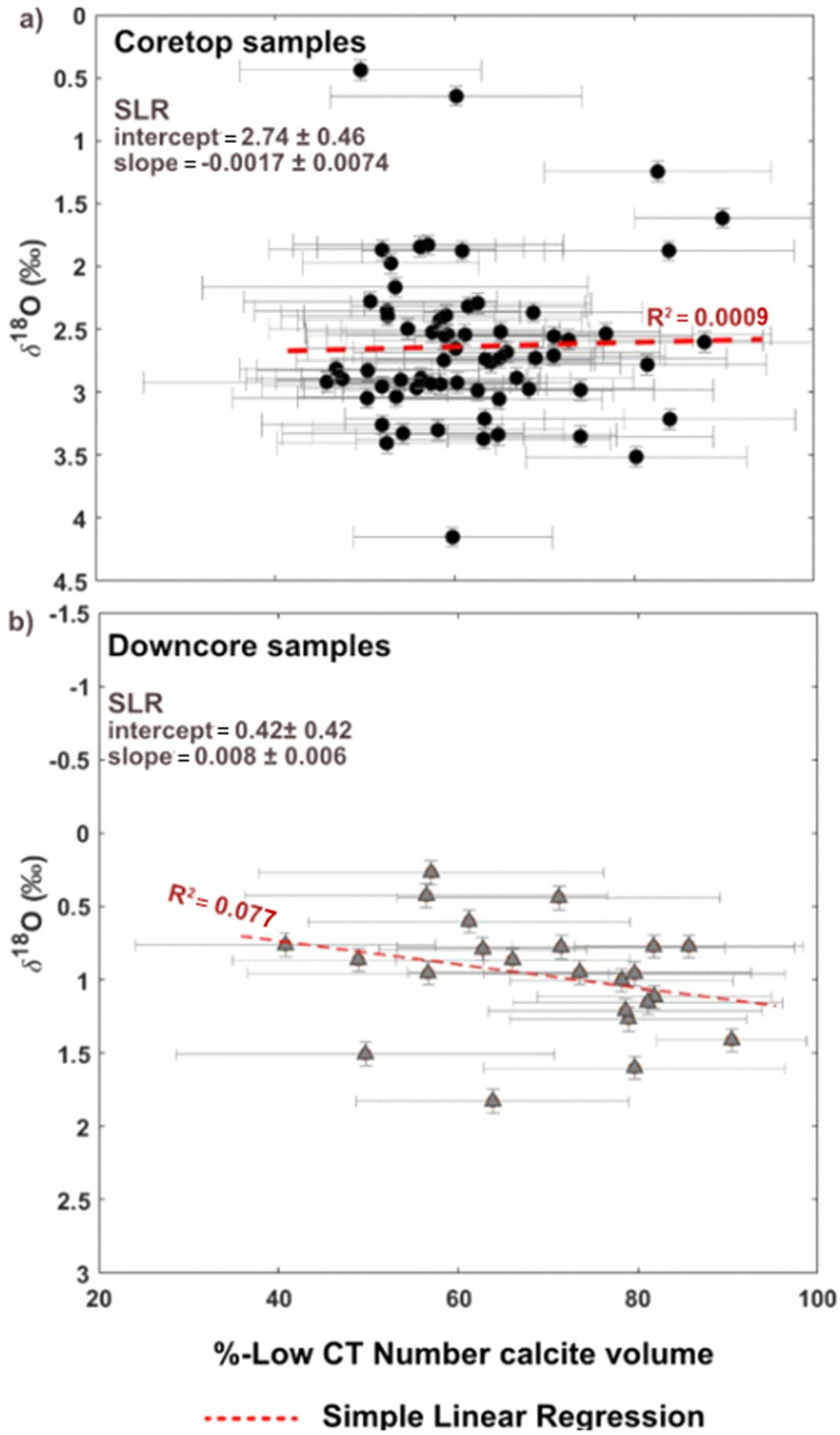

Figure 6. %Low CT Number Calcite volume and $\delta^{18}O$ do not show a significant correlation in either the (a) coretop ($p > 0.1$, Table 2) or (b) downcore populations ($p > 0.1$, Table 2).

to the bulk test (Figure 8), following laboratory culture and dissolution experiments by Spero and Lea (1996). Quantitatively, we find that the direct effect of dissolution likely lowers $\delta^{18}O$ by ~0.1‰ (Figure S8 in Supporting Information S1). The variation observed in $\delta^{18}O$ in our IFA data set, however, is substantially larger (1σ of the coretop population is 0.62‰ and that of the downcore population is 0.38‰). Accordingly, it is unlikely that dissolution alone is responsible for the isotopic variation we observe.

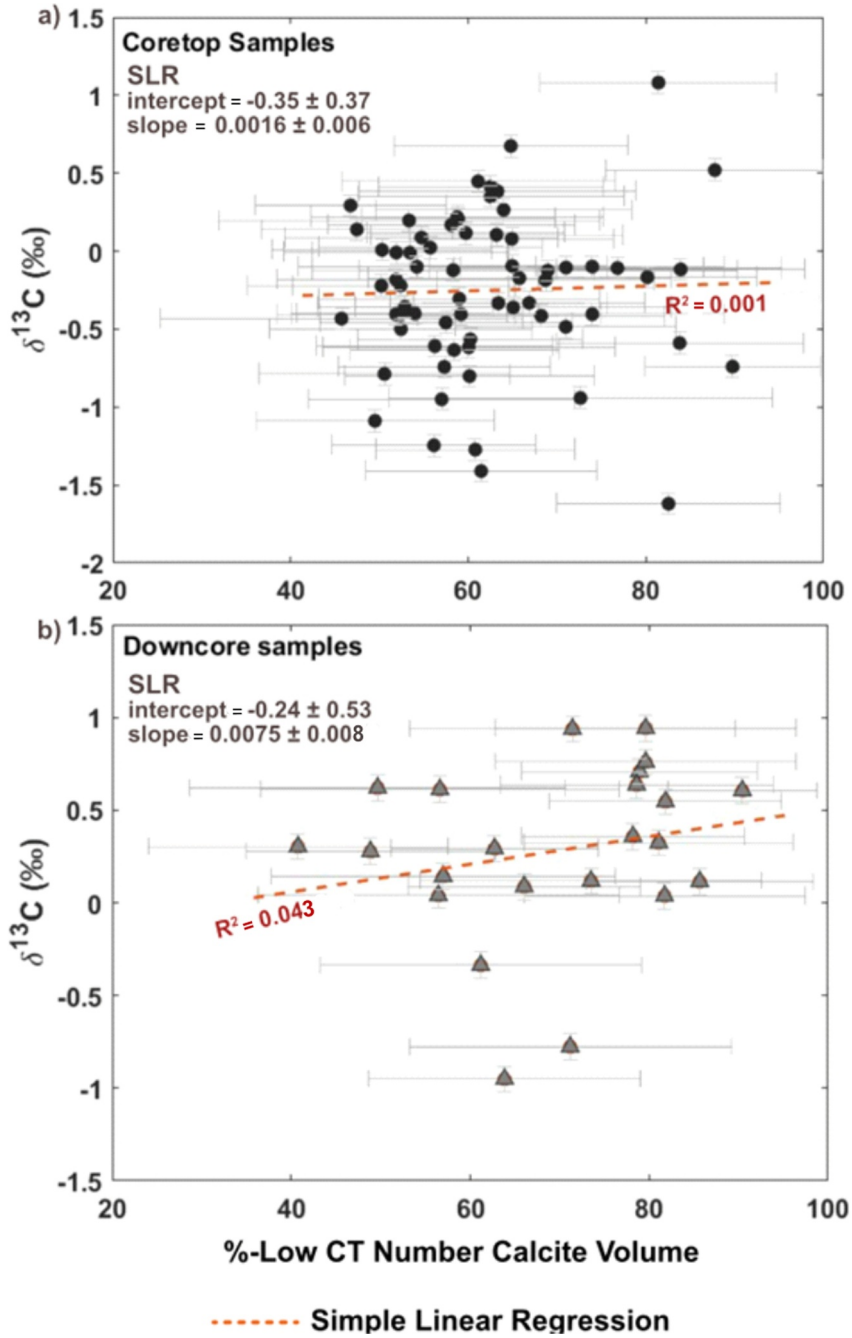

Figure 7. %Low CT Number Calcite volume and $\delta^{13}C$ do not have a significant correlation in either the (a) coretop ($p > 0.5$, Table 3) and (b) downcore populations ($p > 0.5$, Table 3).

Table 2
Parameters for Simple Linear Regression Fit to the %Low CT Calcite Volume Versus $\delta^{18}O$ Data Set

	Intercept	Intercept error	Slope	Slope error	r^2	p
Coretop	2.74	0.46	0.0017	0.0074	0.0009	0.85
Downcore	0.42	0.42	0.0080	0.0060	0.077	0.41

Table 3
Parameters for Simple Linear Regression Fit to the %Low CT Calcite Volume Versus $\delta^{13}C$ Data Set

	Intercept	Intercept error	Slope	Slope error	r^2	p
Coretop	−0.35	0.37	0.0016	0.006	0.001	0.84
Downcore	−0.24	0.53	0.0075	0.008	0.043	0.51

5.3. Drivers of Isotopic Variation Within Populations

Apart from ambient seawater chemistry and temperature, processes operating on diurnal, seasonal or subdecadal timescales can drive large ranges in primary paleoenvironmental signals recorded by foraminifera. Vital effects, or variations in test geochemistry caused by a plethora of biological factors such as differential rates of respiration, calcification, or life stage (Bemis et al., 1998; Naidu & Niitsuma, 2004; Spero & Lea, 1996), may vary between individuals of the same species, and within each individual at different points in its life cycle (Naidu et al., 2019). For example, significant increases in $\delta^{13}C$ and $\delta^{18}O$ in comparison to equilibrium calcite values (by ∼1‰ and ∼2‰ respectively) measured on *G. bulloides* from the Southern Ocean (south of 40°S) have been attributed to disequilibrium calcification driven by vital effects (Prasanna et al., 2016). Similarly, using the calcification depth temperatures of *G. bulloides* (∼13.5–10.5°C between 0 and 200 m; Garcia et al., 2019; Boyer et al., 2018) in the set of calibration equations by Bemis et al. (1998), we find that $\delta^{18}O$ values of *G. bulloides* assuming equilibrium calcification lie between −0.2‰–0.79‰. Whereas this matches the equilibrium calcification ranges from Prasanna et al. (2016), we observed a wider range of $\delta^{18}O$ variability from IFA analysis of our coretop samples, which may be attributed to increased seasonal variations captured by IFA relative to multi-specimen analyses superimposed over the aforementioned vital effect offsets.

Isotopic variation on seasonal timescales is typically captured by monitoring the flux of foraminiferal species to sediment traps and measuring the $\delta^{13}C$ and $\delta^{18}O$ of aliquots made up of multiple foraminifera (King & Howard, 2005; Naik et al., 2014). *G. bulloides* typically reside within the mixed layer or ML (Fairbanks et al., 1980), the depth of which shows marked seasonal variation. This leads to variation in $\delta^{18}O$ related to calcification depth (Lakhani et al., 2022). ML depth and temperatures in the Sub-Tropical Zone (STZ) of the Southern Ocean show seasonal variations (Racape et al., 2010), which are then reflected in the isotopic

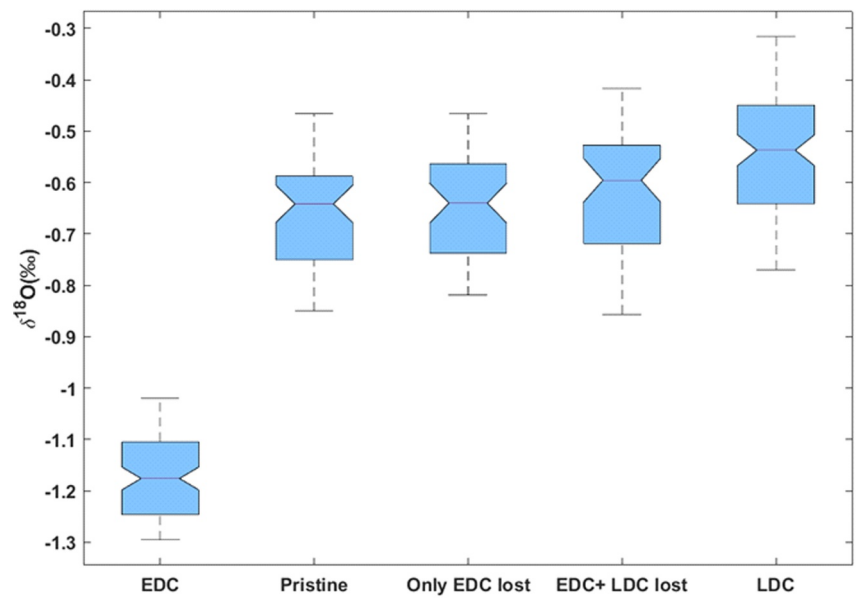

Figure 8. Far left: $\delta^{18}O$ range of early developed calcite forming the nine innermost chambers of *G. bulloides* on the far left and far right: more $\delta^{18}O$-enriched, later developed calcite (LDC) formed deeper in the water column. The 2nd, 3rd, and 4th box plots represent $\delta^{18}O$ ranges of pristine tests, modeled $\delta^{18}O$ values assuming only early-developed calcite (EDC) loss, and modeled $\delta^{18}O$ values assuming both EDC and LDC loss. Initial $\delta^{18}O$ of whole tests, EDC and LDC are taken from Spero and Lea (1996).

compositions of calcite (King & Howard, 2005). *G. bulloides* tests also show fine-scale heterogeneities in $\delta^{18}O$ due to temperature differences associated with varying depths of calcification at various life stages (Spero & Lea, 1996) and represent temperature changes over days or weeks. Thus, these heterogeneities contribute to the variation in IFA isotopic compositions that represent an average value for the entire lifetime of an individual (Figure S7 in Supporting Information S1).

Processes such as vital effects, seasonal variations in temperature or productivity, and transportation by ocean currents might explain the within-population ranges we observe in both our coretop and downcore data sets (Figure 5). Strong seasonal cyclicity in the downward flux of *G. bulloides* tests has been observed across multiple Southern Ocean sites, where the majority of the tests are produced during the austral summer and represent periods of higher productivity and temperatures (Jonkers & Kučera, 2015; King & Howard, 2003, 2005). Variations in $\delta^{18}O$ may also arise due to the transportation of foraminiferal tests from warmer waters at lower latitudes by means of the Agulhas current and Agulhas rings. Depending on their lifespan, foraminifera can drift for several hundreds to >1,000 km, which may introduce offsets of as much as 1.5–3°C in the temperature record, when compared to values calculated assuming vertical settling alone (van Sebille et al., 2015).

Regardless, the lack of correlation between XMCT data and the isotopic measurements implies that, whatever the cause of within-population $\delta^{18}O$ variation, the same drivers do not also affect the extent of test dissolution. This suggests that XMCT and IFA provide orthogonal information about environmental conditions. Interpreted in this way, the lack of correlation suggests that the processes driving differences in dissolution extent over the approximately millennial time scale recorded by each sample are largely decoupled from the temperature variation that affects $\delta^{18}O$ over the same timescales. Though we failed to detect a within-population correlation between CT and isotope data, this does not preclude such a correlation within other sample sets and/or an underlying relationship between dissolution and temperature over millennial timescales that is small in magnitude compared to the other drivers of variability impacting tests at our study site.

Decoupling of the dissolution extent of foraminifera from a calcification signal may occur due to variations in relative proportions of early-developed and later-developed calcite. Based on the life stage at which an individual dies and is deposited, the number of outer chambers formed by the foraminifera varies, and a relatively higher fraction of EDC may be lost. Furthermore, test dissolution extent is time-dependent (Iwasaki et al., 2015). Thus, the time of exposure of foraminifera to corrosive bottom waters likely determines how much mass is lost from tests and, in turn, modulates changes in test density and CT Number distributions. Strong current action can cause erosion at the ocean floor (Beelen & Wood, 2023), exposing foraminifera to a calcite-undersaturated environment; conversely, rapid burial of foraminifera due to higher sedimentation rates can limit the time and extent of dissolution without an obvious dependency on temperature.

5.4. Coupled Changes in Partial Dissolution Extent and Oxygen Isotopic Ratios Over Geologic Timescales

Besides the within-population variations revealed by IFA, we also observe differences between the coretop and downcore populations. These differences can be highlighted using "bulk" values calculated by averaging all the CT data for each population as well as all the isotopic measurements. Since the ranges in percentage of low CT Number calcite volume overlap between the coretop and downcore populations, we use all of the available CT scans to calculate bulk values as opposed to the subset with paired isotopic data. This approach assures the most robust estimate of differences in dissolution extent between the two samples, though our ultimate interpretation is insensitive to this choice. The ranges in $\delta^{18}O$ values from the two samples do not overlap as strongly as in the CT data, such that the smaller number of individuals included in our calculation of bulk values is not expected to substantially influence the results. Moreover, because the %Low CT Number Calcite volume and $\delta^{18}O$ are uncorrelated (Figures 7a and 7b), their respective bulk values should be comparable despite the fact that they are based on different numbers of individual tests.

We find that the downcore population has higher mean and median %Low-CT-number calcite volume relative to coretop samples (Figure 9). As foraminifera undergo dissolution and breakdown of the test ultrastructure occurs, test density decreases, and CT Numbers shift to lower values. Consequently, there is an increase in the %Low-CT-Number calcite volume. Thus, XMCT-based proxies indicate that the downcore population overall shows evidence of greater dissolution.

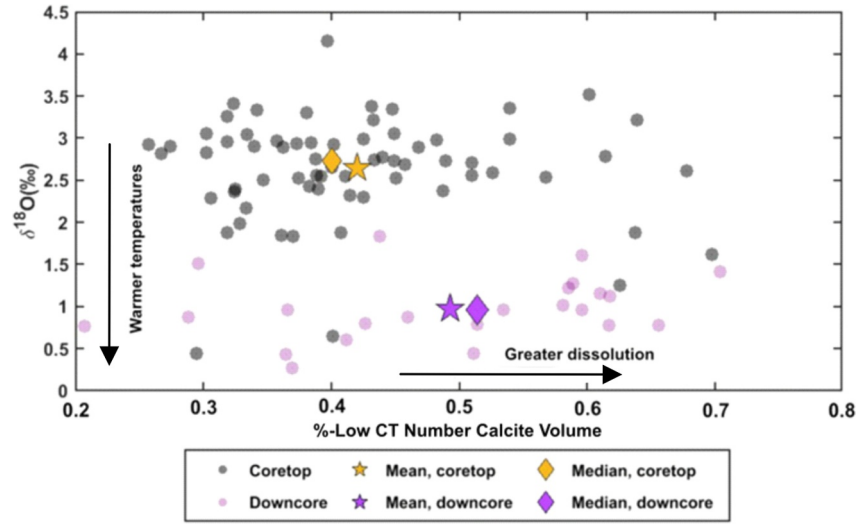

Figure 9. Comparison of IFA and $\delta^{18}O$ statistics of coretop and downcore foraminifera. "Bulk" population statistics of both the coretop and downcore populations, namely means (denoted by stars) and median (denoted by diamonds), indicate overall warmer temperatures and a greater extent of dissolution in the downcore population.

We interpret warmer sea surface temperatures (SSTs) as the cause for the differences with the downcore population based on lower "bulk" (i.e., approximating multi-specimen analysis) mean and median $\delta^{18}O$ values in comparison with the coretop population (Figure 7). The measured oxygen isotopic values in the downcore samples can, in part, be attributed to the lowering in global $\delta^{18}O$ of seawater in the downcore period relative to the coretop interval. However, the difference in $\delta^{18}O_{seawater}$ between the present-day and earliest Pliocene, based on benthic foraminiferal $\delta^{18}O$ records (Westerhold et al., 2020), is ~1.3‰. This is smaller than the 1.78‰ difference between median values of the coretop and downcore populations from Site 1088. The remaining ~0.48‰ difference in $\delta^{18}O$ may be attributed to temperature differences between the two time periods, roughly amounting to ~2°C warmer waters. We note that changes in local $\delta^{18}O_{sw}$ and associated potential changes in water-column salinity may have also contributed to these changes. However, we submit that this effect is small based on modern variations in seawater $\delta^{18}O$ (LeGrande & Schmidt, 2006). Our interpretation of $\delta^{18}O$ differences as reflecting warmer SSTs is consistent with positive SST anomalies at Site 1088 (1088B-6H-5, 50.2 mbsf) derived from the alkenone proxy (Herbert et al., 2016) as well as bulk Mg/Ca of *G. bulloides* (Vautravers, 2014).

Carbonate dissolution is brought about by a lowering of the calcite saturation state of seawater, Ω, which depends, among other variables, on the concentration of carbonate ion ($[CO_3^{2-}]$). Lower seawater $[CO_3^{2-}]$ can be driven by elevated atmospheric pCO_2, which also gives rise to increased SSTs. In this way, geologic changes in atmospheric pCO_2 can drive the coupled changes in test preservation and O isotopic composition, that we observe in our sample set (Figure 9). Although large uncertainties in pCO_2 estimates of the late Messinian exist (Pagani et al., 2005, 2009; Pound et al., 2012; Rae et al., 2021; Steinthorsdottir et al., 2021), there is isotopic evidence of a short-term warming period (superimposed on a longer-term trend of Middle Miocene global cooling) from ~5.5. Ma onwards due to transition from the glacial TG 12 to the interglacial TG 11 stage (Pérez-Asensio et al., 2013; Vautravers, 2014) that may be attributed to higher pCO_2. Despite uncertainties, available pCO_2 reconstructions are consistent with higher values in the Pliocene/Miocene compared to the pre-industrial period (Rae et al., 2021). Higher atmospheric pCO_2 is consistent with a lowering of the calcite saturation state of the ocean, leading to enhanced carbonate dissolution, which matches our observations of differences between the coretop and downcore samples.

6. Conclusion

In this work, we utilize a combined approach of X-ray Micro CT Scanning and individual foraminiferal analysis (IFA) of planktic foraminifera from a site in the sub-Antarctic Southern Ocean to assess the utility of pairing physical and geochemical proxies measured at the level of individual tests. We see evidence of varying degrees of dissolution in the shapes of the CT Number distributions of scanned tests. Left-skewed, unimodal CT Number

distributions with narrow peaks are inferred as signatures of high dissolution intensities based on evidence from prior studies. By looking at the correlation between the CT and isotopic data for individual populations, we find evidence that the factors driving short-term changes in dissolution extent are distinct from those driving changes in temperature over the same timescales. However, by comparing averages for the analyzed coretop and downcore populations, we find evidence of longer-term correlations between oceanographic conditions and foraminiferal preservation consistent with expectations for a high pCO_2 atmosphere (i.e., warmer temperatures and a more acidic ocean).

Data Availability Statement

The dataset for this study and CT number distributions for all scanned foraminifera are available at Zenodo (Jana et al., 2024). Sediment samples from ODP Site 1088 may be obtained from the International Ocean Drilling Program's Gulf Core Repository at Texas A&M University, College Station, Texas. Image processing was done on MATLAB R2023a (The MathWorks Inc. (2023). MATLAB version: 9.13.0 (R2023ab), Natick, Massachusetts: The MathWorks Inc. https://www.mathworks.com). MicroCT data processing was done using 3D Slicer, an open-source software (https://www.slicer.org/). Sitemaps were generated using OceanDataView (ODV), which is available at https://explore.webodv.awi.de/ (Schlitzer, 2015).

Acknowledgments
We would like to acknowledge the valuable input from Dr. Ashley Burkett, Dr. Udayabhanu Jammalamadaka, Dr. Olivier LaRouche, and Sean Trainor, who were instrumental in setting up the X-ray Micro CT Scanning workflow, and Dr. Tao Sun for his help with stable isotope measurements. Members of the Paleo^2 Lab at the University of Arizona are acknowledged for their assistance in the IFA measurements. DJ acknowledges salary support through IODP Expedition 392 Post Expedition Award (PEA). KT acknowledges support from NSF OCE 2423147.

References

Adkins, J. F., Naviaux, J. D., Subhas, A. V., Dong, S., & Berelson, W. M. (2021). The dissolution rate of $CaCO_3$ in the ocean. *Annual Review of Marine Science*, *13*(January), 57–80. https://doi.org/10.1146/annurev-marine-041720-092514

Bé, A. W. H., & Hamlin, W. H. (1967). Ecology of recent planktonic foraminifera: Part 3: Distribution in the North Atlantic during the summer of 1962. *Micropaleontology*, *13*(1), 87–106. https://doi.org/10.2307/1484808

Bé, A. W. H., Morse, J. W., & Harrison, S. M. (1975). *Progressive dissolution and ultrastructural breakdown of planktonic foraminifera*. pubs.geoscienceworld.org. Retrieved from https://pubs.geoscienceworld.org/cushmanfoundation/books/book/2237/chapter-pdf/5013864/sp13_ch03.pdf

Beelen, D., & Wood, L. J. (2023). Predicting bottom current deposition and erosion on the ocean floor. *Basin Research*, *35*(5), 1985–2009. https://doi.org/10.1111/bre.12788

Bemis, B. E., Howard, J. S., Bijma, J., & David, W. L. (1998). Reevaluation of the oxygen isotopic composition of planktonic foraminifera: Experimental results and revised paleotemperature equations. *Paleoceanography and Paleoclimatology*, *13*(2), 150–160.

Billups, K. (2002). Late Miocene through early Pliocene deep water circulation and climate change viewed from the sub-Antarctic south Atlantic. *Palaeogeography, Palaeoclimatology, Palaeoecology*, *185*(3), 287–307. https://doi.org/10.1016/s0031-0182(02)00340-1

Boudreau, B. P., Middelburg, J. J., & Luo, Y. (2018). The role of calcification in carbonate compensation. *Nature Geoscience*, *11*(12), 894–900. https://doi.org/10.1038/s41561-018-0259-5

Boyer, T. T. P., Garcia, H. E., Locarnini, R. A., Zweng, M. M., Mishonov, A. V., Reagan, J. R., et al. (2018). World Ocean Atlas 2018 [Dataset]. *NOAA National Centers for Environmental Information*. Retrieved from https://www.ncei.noaa.gov/archive/accession/NCEI-WOA18

Broecker, W. S., & Takahashi, T. (1978). The relationship between Lysocline depth and in Situ carbonate ion concentration* *Lamont-Doherty geological observatory contribution No. 2584.† †GEOSECS Publication No. 61. *Deep Sea Research Part I: Oceanographic Research Papers*, *25*(1), 65–95. https://doi.org/10.1016/s0146-6291(21)00007-2

Bruker Corporation. (2024). Bruker nRecon-reconstruction-software [Software]. *Bruker Corporation*. Retrieved from https://www.microphotonics.com/micro-ct-systems/nrecon-reconstruction-software/

Burke, J. E., Renema, W., Henehan, M. J., Elder, L. E., Davis, C. V., Maas, A. E., et al. (2018). Factors influencing test porosity in planktonic foraminifera. *Biogeosciences*, *15*(21), 6607–6619. https://doi.org/10.5194/bg-15-6607-2018

Clemens, S. C., Thirumalai, K., & Oppo, D. (2023). Indian margin methane hydrate dissociation recorded in the carbon isotopes of benthic (Miliolida) foraminifera. *Earth and Planetary Science Letters*, *609*, 11801. https://doi.org/10.1016/j.epsl.2023.118101

Davis, C. V., Wishner, K., Renema, W., & Hull, P. M. (2021). Vertical distribution of planktic foraminifera through an oxygen Minimum zone: How assemblages and test morphology reflect oxygen concentrations. *Biogeosciences*, *18*(3), 977–992. https://doi.org/10.5194/bg-18-977-2021

Emiliani, C. (1955). Pleistocene temperatures. *The Journal of Geology*, *63*(6), 538–578. https://doi.org/10.1086/626295

Erez, J., & Luz, B. (1983). Experimental paleotemperature equation for planktonic foraminifera. *Geochimica et Cosmochimica Acta*, *47*(6), 1025–1031. https://doi.org/10.1016/0016-7037(83)90232-6

Fairbanks, R. G., Wiebe, P. H., & Bé, A. W. (1980). Vertical distribution and isotopic composition of living planktonic foraminifera in the Western North Atlantic. *Science*, *207*(4426), 61–63. https://doi.org/10.1126/science.207.4426.61

Fedorov, A., Beichel, R., Kalpathy-Cramer, J., Finet, J., Fillion-Robin, J.-C., Pujol, S., et al. (2012). 3D slicer as an image computing platform for the quantitative imaging network [Software]. *Magnetic Resonance Imaging*, *30*(9), 1323–1341. https://doi.org/10.1016/j.mri.2012.05.001

Feely, R. A., Sabine, C. L., Lee, K., Berelson, W., Kleypas, J., Fabry, V. J., & Millero, F. J. (2004). Impact of anthropogenic CO_2 on the $CaCO_3$ system in the oceans. *Science*, *305*(5682), 362–366. https://doi.org/10.1126/science.1097329

Ford, H. L., Christina Ravelo, A., & Polissar, P. J. (2015). Reduced El Niño-southern Oscillation during the last glacial maximum. *Science*, *347*(6219), 255–258. https://doi.org/10.1126/science.1258437

Garcia, H. E., Boyer, T. P., Baranova, O. K., Locarnini, R. A., Mishonov, A. V., Grodsky, A., et al. (2019). World ocean atlas 2018: Product documentation.

Gersonde, R., Hodell, D., & Blum, P. (1998). Southern Ocean Paleoceanography. In *ODP Preliminary report*. https://doi.org/10.2973/odp.pr.177.1998

Glaubke, R. H., Thirumalai, K., Schmidt, M. W., & Hertzberg, J. E. (2021). Discerning changes in high-frequency climate variation using geochemical populations of individual foraminifera. *Paleoceanography and Paleoclimatology*, *36*(2), e2020PA004065. https://doi.org/10.1029/2020pa004065

Glock, N., Eisenhauer, A., Milker, Y., Liebetrau, V., Schönfeld, J., Mallon, J., et al. (2011). Environmental influences on the pore density of Bolivina Spissa (Cushman). *Journal of Foraminiferal Research*, *41*(1), 22–32. https://doi.org/10.2113/gsjfr.41.1.22

Gruetzner, J., Uenzelmann-Neben, G., & Franke, D. (2016). Evolution of the Northern Argentine margin during the Cenozoic controlled by bottom current dynamics and Gravitational processes. *Geochemistry: Exploration, Environment, Analysis*, *17*(8), 3131–3149. https://doi.org/10.1002/2015GC006232

Hayes, C. T., Costa, K. M., Anderson, R. F., Calvo, E., Chase, Z., Demina, L. L., et al. (2021). Global Ocean sediment composition and burial flux in the deep sea. *Global Biogeochemical Cycles*, *35*(4), e2020GB006769. https://doi.org/10.1029/2020gb006769

Hemleben, C., Spindler, M., & Roger Anderson, O. (2012). *Modern planktonic foraminifera*. Springer Science & Business Media.

Herbert, T. D., Lawrence, K. T., Tzanova, A., Peterson, L. C., Caballero-Gill, R., & Kelly, C. S. (2016). Late Miocene global cooling and the rise of modern Ecosystems. *Nature Geoscience*, *9*(11), 843–847. https://doi.org/10.1038/ngeo2813

Hodell, D. A., Charles, C. D., Curtis, J. H., Mortyn, P. G., Ninnemann, U. S., & Venz, K. A. (2003). Data Report: Oxygen isotope stratigraphy of ODP Leg 177 sites 1088, 1089, 1090, 1093, and 1094. *Proceedings of the Ocean Drilling Program, Scientific Results*, *177*, 1–26. Retrieved from www-odp.tamu.edu

Hönisch, B., Ridgwell, A., Schmidt, D. N., Thomas, E., Gibbs, S. J., Sluijs, A., et al. (2012). The geological record of ocean Acidification. *Science*, *335*(6072), 1058–1063. https://doi.org/10.1126/science.1208277

Iwasaki, S., Kimoto, K., & Kucera, M. (2023). Development of a deep-water carbonate ion concentration proxy based on preservation of planktonic foraminifera shells Quantified by X-ray CT scanning. *Paleoceanography and Paleoclimatology*, *38*(8), e2022PA004601. https://doi.org/10.1029/2022pa004601

Iwasaki, S., Kimoto, K., Okazaki, Y., & Ikehara, M. (2019). Micro-CT scanning of tests of three planktic foraminiferal species to Clarify DissolutionProcess and progress. *Geochemistry, Geophysics, Geosystems*, *20*(12), 6051–6065. https://doi.org/10.1029/2019gc008456

Iwasaki, S., Kimoto, K., Sasaki, O., Kano, H., Honda, M. C., & Okazaki, Y. (2015). Observation of the dissolution process of Globigerina bulloides tests (planktic foraminifera) by X-ray Microcomputed Tomography. *Paleoceanography*, *30*(4), 317–331. https://doi.org/10.1002/2014pa002639

Jana, D., Torres, M., Evans, K., K Jayan, A., & Thirumalai, K. (2024). Paired X-ray Micro CT Scanning and individual foraminifera isotopic analysis reveal (de)coupled changes in carbonate preservation and temperature [Dataset]. *Zenodo*. https://doi.org/10.5281/zenodo.13755262

Johnstone, H. J. H., Jimin, Y., Henry, E., & Schulz, M. (2011). Improving temperature estimates derived from Mg/Ca of planktonic foraminifera using X-ray Computed Tomography–based dissolution Index, XDX. *Paleoceanography*, *26*(1), PA1215. https://doi.org/10.1029/2009pa001902

Johnstone, H. J. H., Schulz, M., Barker, S., & Elderfield, H. (2010). Inside story: An X-ray computed tomography method for assessing dissolution in the tests of planktonic foraminifera. *Marine Micropaleontology*, *77*(1), 58–70. https://doi.org/10.1016/j.marmicro.2010.07.004

Jonkers, L., & Kučera, M. (2015). Global analysis of seasonality in the shell flux of extant planktonic Foraminifera. *Biogeosciences*, *12*(7), 2207–2226. https://doi.org/10.5194/bg-12-2207-2015

Jonkers, L., van Heuven, S., Zahn, R., & Peeters, F. J. C. (2013). Seasonal Patterns of shell flux, $\delta^{18}O$ and $\delta^{13}C$ of small and large *N. pachyderma* (s) and *G. bulloides* in the Subpolar North Atlantic. *Paleoceanography*, *28*(1), 164–174. https://doi.org/10.1002/palo.20018

Khider, D., Stott, L. D., Emile-Geay, J., Thunell, R., & Hammond, D. E. (2011). Assessing El Niño southern Oscillation variability during the past Millennium. *Paleoceanography*, *26*(3), PA3222. https://doi.org/10.1029/2011pa002139

Killingley, J. S., Johnson, R. F., & Berger, W. H. (1981). Oxygen and carbon isotopes of individual shells of planktonic foraminifera from Ontong-Java plateau, Equatorial Pacific. *Palaeogeography, Palaeoclimatology, Palaeoecology*, *33*(1), 193–204. https://doi.org/10.1016/0031-0182(81)90038-9

King, A. L., & Howard, W. R. (2003). Planktonic foraminiferal flux seasonality in Subantarctic sediment traps: A test for paleoclimate reconstructions. *Paleoceanography*, *18*(1), 1019. https://doi.org/10.1029/2002pa000839

King, A. L., & Howard, W. R. (2005). $\delta^{18}O$ seasonality of planktonic foraminifera from Southern Ocean sediment traps: Latitudinal Gradients and implications for paleoclimate reconstructions. *Marine Micropaleontology*, *56*(1), 1–24. https://doi.org/10.1016/j.marmicro.2005.02.008

Kuroyanagi, A., da Rocha, R. E., Bijma, J., Spero, H. J., Russell, A. D., Eggins, S. M., & Kawahata, H. (2013). Effect of dissolved oxygen concentration on planktonic foraminifera through laboratory culture experiments and implications for oceanic Anoxic Events. *Marine Micropaleontology*, *101*(May), 28–32. https://doi.org/10.1016/j.marmicro.2013.04.005

Lakhani, K. Q., Lynch-Stieglitz, J., & Monteagudo, M. M. (2022). Constraining calcification habitat using oxygen isotope measurements in tropical planktonic foraminiferal tests from surface sediments. *Marine Micropaleontology*, *170*, 102074. https://doi.org/10.1016/j.marmicro.2021.102074

LeGrande, A. N., & Schmidt, G. A. (2006). Global Gridded data set of the oxygen isotopic composition in seawater. *Geophysical Research Letters*, *33*, L12604. https://doi.org/10.1029/2006GL026011

Lohmann, G. P. (1995). A model for variation in the chemistry of planktonic foraminifera due to Secondary calcification and Selective dissolution. *Paleoceanography*, *10*(3), 445–457. https://doi.org/10.1029/95pa00059

Marino, M., & Flores, J. A. (2002). Miocene to Pliocene calcareous nannofossil biostratigraphy at ODP Leg 177 sites 1088 and 1090. *Marine Micropaleontology*, *45*(3–4), 291–307. https://doi.org/10.1016/s0377-8398(02)00033-6

Metcalfe, B., Lougheed, B. C., Waelbroeck, C., & Roche, D. M. (2019). On the Validity of foraminifera-based ENSO reconstructions. In *Climate of the past discussions* (pp. 1–31).

Milliman, J. D. (1993). Production and Accumulation of calcium carbonate in the ocean: Budget of a nonsteady state. *Global Biogeochemical Cycles*, *7*(4), 927–957. https://doi.org/10.1029/93gb02524

Naidu, P. D., & Niitsuma, N. (2004). Atypical δ13C Signature in Globigerina Bulloides at the ODP Site 723A (Arabian Sea): Implications of Environmental Changes Caused by Upwelling. *Marine Micropaleontology*, *53*(1), 1–10. https://doi.org/10.1016/j.marmicro.2004.01.005

Naidu, P. D., Niitsuma, N., Thirumalai, K., & Naik, S. S. (2019). Significant Seasonal Contrast in the Arabian Sea during Deglaciation: Evidence from Oxygen Isotopic Analyses of Individual Planktic Foraminifera. *Quaternary International: The Journal of the International Union for Quaternary Research*, *503*(February), 163–169. https://doi.org/10.1016/j.quaint.2018.08.005

Naik, D. K., Saraswat, R., Khare, N., Pandey, A. C., & Nigam, R. (2014). Hydrographic changes in the Agulhas Recirculation Region during the Late Quaternary. *Climate of the Past*, *10*(2), 745–758. https://doi.org/10.5194/cp-10-745-2014

Pagani, M., Liu, Z., LaRiviere, J., & Ravelo, A. C. (2009). High Earth-system climate sensitivity determined from Pliocene carbon dioxide concentrations. *Nature Geoscience*, *3*(1), 27–30. https://doi.org/10.1038/ngeo724

Pagani, M., Zachos, J. C., Freeman, K. H., Tipple, B., & Bohaty, S. (2005). Marked decline in atmospheric carbon dioxide concentrations during the Paleogene. *Science*, *309*(5734), 600–603. https://doi.org/10.1126/science.1110063

Pak, D. K., Lea, D. W., & Kennett, J. P. (2004). Seasonal and interannual variation in Santa Barbara basin water temperatures observed in sediment trap foraminiferal Mg/Ca. *Geochemistry, Geophysics, Geosystems*, *5*(12), Q12008. https://doi.org/10.1029/2004gc000760

Pérez-Asensio, J. N., Aguirre, J., Jiménez-Moreno, G., Schmiedl, G., & Civis, J. (2013). Glacioeustatic control on the origin and cessation of the Messinian salinity crisis. *Global and Planetary Change*, *111*(December), 1–8. https://doi.org/10.1016/j.gloplacha.2013.08.008

Pound, M. J., Haywood, A. M., Ulrich, S., & Riding, J. B. (2012). Global vegetation dynamics and latitudinal temperature gradients during the Mid to Late Miocene (15.97–5.33 Ma). *Earth-Science Reviews*, *112*(1), 1–22. https://doi.org/10.1016/j.earscirev.2012.02.005

Prasanna, K., Ghosh, P., Bhattacharya, S. K., Mohan, K., & Anilkumar, N. (2016). Isotopic disequilibrium in *Globigerina bulloides* and carbon isotope response to productivity increase in Southern Ocean. *Scientific Reports*, *6*(February), 21533. https://doi.org/10.1038/srep21533

Racapé, V., Monaco, L., Metzl, N., & Pierre, C. (2010). Summer and winter distribution of δ^{13}CDIC in surface waters of the South Indian Ocean [20°S–60°S]. *Tellus Series B Chemical and Physical Meteorology*, *62*(5), 660–673. https://doi.org/10.3402/tellusb.v62i5.16618

Rae, J. W. B., Zhang, Y. G., Liu, X., Foster, G. L., Stoll, H. M., & Whiteford, R. D. M. (2021). Atmospheric CO_2 over the past 66 million years from Marine Archives. *Annual Review of Earth and Planetary Sciences*, *49*(1), 609–641. https://doi.org/10.1146/annurev-earth-082420-063026

Ravelo, A. C., & Hillaire-Marcel, C. (2007). Chapter Eighteen: The use of oxygen and carbon isotopes of foraminifera in paleoceanography. In C. Hillaire-Marcel & A. De Vernal (Eds.), *Developments in marine geology* (Vol. 1, pp. 735–764). Elsevier. https://doi.org/10.1016/s1572-5480(07)01023-8

Regenberg, M., Regenberg, A., Garbe-Schönberg, D., & Lea, D. W. (2014). Global dissolution effects on planktonic foraminiferal Mg/Ca ratios controlled by the calcite-saturation state of bottom waters. *Paleoceanography*, *29*(3), 127–142. https://doi.org/10.1002/2013pa002492

Sadekov, A. Y., Ganeshram, R., Pichevin, L., Rose, B., McClymont, E., Henry, E., & Tudhope, A. W. (2013). Palaeoclimate reconstructions reveal a strong link between El Niño-southern oscillation and tropical pacific mean state. *Nature Communications*, *4*(1), 2692. https://doi.org/10.1038/ncomms3692

Schiebel, R., Bijma, J., & Hemleben, C. (1997). Population dynamics of the planktic foraminifer Globigerina bulloides from the eastern North Atlantic. *Deep-Sea Research Part A Oceanographic Research Papers*, *44*(9–10), 1701–1713. https://doi.org/10.1016/s0967-0637(97)00036-8

Schlitzer, R. (2015). Data Analysis and Visualization with Ocean Data View [Software]. *CMOS Bulletin SCMO*, *43*(1), 9–13. Retrieved from https://epic.awi.de/id/eprint/37570/

Scotese, C. R., Song, H., Mills, B. J. W., & van der Meer, D. G. (2021). Phanerozoic paleotemperatures: The Earth's changing climate during the last 540 million years. *Earth-Science Reviews*, *215*(103503), 103503. https://doi.org/10.1016/j.earscirev.2021.103503

SenGupta, B. K. (2002). *Modern foraminifera*. Kluwer Academic Publishers.

Shackleton, N. J. (1987). Oxygen isotopes, ice volume and sea level. *Quaternary Science Reviews*, *6*(3), 183–190. https://doi.org/10.1016/0277-3791(87)90003-5

Shackleton, N. J., & Opdyke, N. D. (1973). Oxygen isotope and palaeomagnetic stratigraphy of Equatorial Pacific core V28-238: Oxygen isotope temperatures and ice volumes on a 105 year and 106 year scale. *Quaternary Research*, *3*(1), 39–55. https://doi.org/10.1016/0033-5894(73)90052-5

Spero, H. J. (1998). Life history and stable isotope geochemistry of planktonic foraminifera. *Paleontological Society Papers*, *4*, 7–36. https://doi.org/10.1017/s1089332600000383

Spero, H. J., & Lea, D. W. (1996). Experimental determination of stable isotope variability in Globigerina bulloides: Implications for paleoceanographic reconstructions. *Marine Micropaleontology*, *28*(3), 231–246. https://doi.org/10.1016/0377-8398(96)00003-5

Steinthorsdottir, M., Coxall, H. K., de Boer, A. M., Huber, M., Barbolini, N., Bradshaw, C. D., et al. (2021). The Miocene: The future of the past. *Paleoceanography and Paleoclimatology*, *36*(4), e2020PA004037. https://doi.org/10.1029/2020pa004037

The MathWorks Inc. (2023). MATLAB version: 9.13.0 (R2023ab), Natick, Massachusetts [Software]. *The MathWorks Inc*. Retrieved from https://www.mathworks.com

Thirumalai, K., & Clemens, S. C. (2020). Monsoon reconstructions using bulk and individual foraminiferal analyses in marine sediments offshore India. *Current Science*, *119*(2), 328. https://doi.org/10.18520/cs/v119/i2/328-334

Thirumalai, K., Cohen, A. S., & Taylor, D. (2023). Hydrologic controls on individual ostracode stable isotopes in a Desert Lake: A modern baseline for Lake Turkana. *Geochemistry, Geophysics, Geosystems*, *24*(5), e2022GC010790. https://doi.org/10.1029/2022gc010790

Thirumalai, K., & Maupin, C. R. (2023). Chasing interannual marine paleovariability. *Paleoceanography and Paleoclimatology*, *38*(8), e2023PA004723. https://doi.org/10.1029/2023pa004723

Thirumalai, K., Partin, J. W., Jackson, C. S., & Quinn, T. M. (2013). Statistical Constraints on El Niño Southern Oscillation Reconstructions Using Individual Foraminifera: A Sensitivity Analysis. *Paleoceanography*, *28*(3), 401–412. https://doi.org/10.1002/palo.20037

Thirumalai, K., Singh, A., & Ramesh, R. (2011). A MATLAB code to perform weighted linear regression with (correlated or uncorrelated) errors in bivariate data. *Journal of the Geological Society of India*, *77*(4), 377–380. https://doi.org/10.1007/s12594-011-0044-1

van Sebille, E., Biastoch, A., van Leeuwen, P. J., & de Ruijter, W. P. M. (2009). A weaker Agulhas Current leads to more Agulhas leakage. *Geophysical Research Letters*, *36*(3), L03601. https://doi.org/10.1029/2008gl036614

van Sebille, E., Scussolini, P., Durgadoo, J. V., Peeters, F. J. C., Biastoch, A., Weijer, W., et al. (2015). Ocean currents generate large footprints in marine palaeoclimate proxies. *Nature Communications*, *6*(1), 6521. https://doi.org/10.1038/ncomms7521

Vautravers, M. J. (2014). Insight into the latest Messinian (5.7–5.2 Ma) palaeoclimatic events from two deep-sea Atlantic Ocean ODP Sites. *Palaeogeography, Palaeoclimatology, Palaeoecology*, *407*(August), 14–24. https://doi.org/10.1016/j.palaeo.2014.03.039

Veizer, J., & Prokoph, A. (2015). Temperatures and oxygen isotopic composition of Phanerozoic oceans. *Earth-Science Reviews*, *146*, 92–104. https://doi.org/10.1016/j.earscirev.2015.03.008

Volbers, A. N. A., & Henrich, R. (2002). Present water mass calcium carbonate corrosiveness in the eastern South Atlantic inferred from ultrastructural breakdown of Globigerina bulloides in surface sediments. *Marine Geology*, *186*(3–4), 471–486. https://doi.org/10.1016/s0025-3227(02)00333-x

Westerhold, T., Marwan, N., Drury, A. J., Liebrand, D., Agnini, C., Anagnostou, E., et al. (2020). An astronomically dated record of Earth's climate and its predictability over the last 66 million years. *Science*, *369*(6509), 1383–1387. https://doi.org/10.1126/science.aba6853

Zarkogiannis, S. D., Iwasaki, S., Rae, J. W. B., Schmidt, M. W., Graham Mortyn, P., George, K., et al. (2022). Calcification, dissolution and test properties of modern planktonic foraminifera from the central Atlantic Ocean. *Frontiers in Marine Science*, *9*, 864801. https://doi.org/10.3389/fmars.2022.864801

Zeebe, R. E., & Wolf-Gladrow, D. (2001). *CO_2 in seawater: Equilibrium, kinetics, isotopes*. Gulf Professional Publishing.